ACTA IMEKO
ISSN: 2221-870X
September 2025, Volume 14, Number 3, 1 - 14

Exploring the interplay of multi-scale climatic variables and forest thinning: From global models to microsite conditions in Northwestern Patagonia

Santiago Varela[1], Juan Pablo Diez[1], Mariana Weigandt[1], Emilio Bianchi[2], Marcos Nacif[3], Lucas A. Garibaldi[3], Octavio Augusto Bruzzone[4]

[1] *Instituto de Investigaciones Forestales y Agropecuaria Bariloche, Instituto Nacional de Tecnología Agropecuaria/ Consejo Nacional de Investigaciones Científicas y Técnicas, San Carlos de Bariloche, Río Negro, Argentina*
[2] *Centro Interdisciplinario de Telecomunicaciones, Electrónica, Computación y Ciencia Aplicada. Universidad Nacional de Río Negro, San Carlos de Bariloche, Río Negro, Argentina*
[3] *Instituto de Investigaciones en Recursos Naturales, Agroecología y Desarrollo Rural, Consejo Nacional de Investigaciones Científicas y Técnicas/Universidad Nacional de Río Negro, San Carlos de Bariloche, Río Negro, Argentina*
[4] *Instituto de Investigaciones en Biodiversidad y Medioambiente (Consejo Nacional de Investigaciones Científicas y Técnicas - Universidad Nacional del Comahue), Rio Negro, Argentina*

ABSTRACT
This research evaluates the influence of site conditions (altitude, slope, and exposure) on air temperature, relative humidity (RH), and vapor pressure deficit (VPD) across two distinct sites and four locations within these. Weather station registers were compared with regional estimates from the ERA5 global model. At two locations in one of these sites, microsite conditions were further analysed under varying thinning intensities, using thermohygrometers. To explore daily cycles, a 24-hour band-pass filter using a Gabor wavelet was applied, calculating weighted averages, amplitudes, and phase shifts. Confidence intervals were derived through Monte Carlo simulations to facilitate robust comparisons across treatments and locations. Observations from weather stations revealed significant discrepancies with ERA5 model estimates, highlighting the limitations of the ERA5 model in capturing fine-scale microclimatic variability driven by local topography and vegetation cover. In south-facing slopes, intensive thinning increased air temperature by 2.5 °C and decreased RH by 12 %, resulting in a midday VPD increase of 0.3 kPa. On north-facing slopes, these effects were less pronounced, with air temperature increases of 1.8 °C and RH decreases of 8 %. Thinning effects were amplified in steeper areas and during summer months. Daily cycle analyses revealed that thinning treatments not only increased amplitude but also caused phase shifts in air temperature and RH, particularly in open areas. These findings underscore the importance of integrating local topographic features, thinning-induced microclimatic changes, and the limitations of ERA5 data into adaptive management frameworks.

Section: RESEARCH PAPER

Keywords: forest thinning intensities; mixed forests; sustainable management

Citation: S. Varela, J. P. Diez, M. Weigandt, E. Bianchi, M. Nacif, L. A. Garibaldi, O. A. Bruzzone, Exploring the interplay of multi-scale climatic variables and forest thinning: From global models to microsite conditions in Northwestern Patagonia, Acta IMEKO, vol. 14 (2025) no. 3, pp. 1-14. DOI: 10.21014/actaimeko.v14i3.2050

Section Editor: Octavian Adrian Postolache, Instituto de Telecomunicações Aveiro, Portugal

Received February 25, 2025; **In final form** July 31, 2025; **Published** September 2025

Funding: This study was conducted without external funding. The data supporting the findings of this study are available upon reasonable request from the corresponding author. The authors declare no competing interests related to this manuscript.

Corresponding author: Santiago Varela, e-mail: varela.santiago@inta.gob.ar

1. INTRODUCTION

In the context of global climate change, the use of models to project the impacts of evolving environmental conditions on the spatiotemporal distribution of plant species has garnered considerable attention in recent decades [1], [2]. These models often rely on climatological data obtained from standardized weather stations, the aim of which is to record regional

meteorological variations and not microclimatic perturbations [3]. Whenever site-specific meteorological data are unavailable, global reanalysis models, such as ERA5, are frequently employed [4], [5]. However, generalized data may misrepresent the fine-scale variability critical for species inhabiting near-ground levels, topographically complex terrains, or forested environments, particularly during early regeneration stages [6]. Forest microclimates, distinct from external climatic conditions, play a pivotal role in shaping tree recruitment, sapling survival, and ecosystem functionality [7], [8], [9], [10]. Although the analysis of the mean values of a climatic series (e.g., temperature) provides valuable insights into general trends, the interpretation of the amplitude and phase of these variables is equally critical, as they reveal temporal and spatial variability patterns that influence ecological and physiological processes [11]. These additional layers of analysis are crucial for robust climate-ecology relationships and effective environmental management strategies.

Deforestation, forest degradation, and fragmentation threaten these microclimatic conditions, exacerbated by climate change, which increases the frequency of severe droughts and alters forest dynamics [10], [12], [13], [14], [15]. Thinning practices, as a forest management tool, influence canopy structure and thus microclimate, offering a potential strategy to enhance forest resilience interactions [16], [17], [18], [19], [20].

Patagonian forests constitute an extensive reservoir of wildlife and a system with great productive potential [21], [22]. Originally, high forests have suffered profound anthropic disturbances and replacement by plantations of exotic conifers, without knowing in detail the impacts of such disturbances [23], [24], [25]. Although these systems have a great capacity for productive improvement, they nonetheless show a growing degradation associated with the lack of knowledge of their real potential [24], making it difficult to reach a consensus on the best practices to apply. In many cases, information regarding the functioning and dynamics of these forests at the community level, and even fundamental features of tree functioning at the individual level, is scarce – elements which are necessary to propose adequate management practices under current climate change.

This study investigates global, regional, site-specific, and microsite climatic patterns in mixed-temperate forests of Northern Patagonia. We assess air temperature, relative humidity (RH), and vapor pressure deficit (VPD) across four sites with varying altitude, slope, and exposure, while analysing microsite conditions under four thinning intensities. By integrating global models with local observations, this research aims to unravel the complex interplay between climatic patterns and thinning practices, informing sustainable management under changing climate conditions.

2. MATERIAL AND METHODS

2.1. Study sites

The study was carried out at two sites (Foyel and Chucao; Table 1) under a mixed low forest condition. The sites were located approximately 80 km south of San Carlos de Bariloche, in the province of Río Negro, Patagonia, Argentina (41° 9´0´´ S, 71° 18´0´´ W). Each forest represents a different stage of the low mixed forest, resulting from the degradation of the high forests of *Nothofagus dombeyi* (coihue). In this region, the climate is temperate-cold, with the highest rainfall being in autumn and winter. The annual precipitation varied between 920 mm and 1300 mm per year [26], [27]. Mean annual air temperature ranged from 8 °C to 9 °C, with mean annual maximum temperatures of 15 °C and minimum of 1.5 °C, mean annual relative humidity was 65 %; frosts were present on average over 120 days a year [28], [29].

2.2. Silvicultural treatments

During May of 2013, four increasing levels of thinning intensity were applied to eight plots (31.5 m × 45.0 m; two plots for each thinning intensity level) at the Foyel site, considering two slope aspects (north and south). The plots were aligned (east-west), with approximately 30 m separating them. Treatments of thinning intensities were quantified as the percentage of basal area removed (30 %, 50 %, and 70 %). Thinning was conducted in strips of varying widths according to the thinning intensities, covering the entire plot. In the plot with 30 % intensity, the six strips had a width of 1.5 m (leaving a 3.0 m space for intact vegetation on the sides). In the plot with 50 % intensity, the six strips had a width of 2.5 m (with the remaining vegetation being 2.0 m wide). Finally, in the plot with 70 % intensity, the six strips had a width of 3.5 m (with the remaining vegetation being 1.0 m wide). In the control plot, vegetation was left uncut (0 % removal). Within the strips, all trees and shrubs were cut with chainsaws and brush cutters at ground level, allowing them the possibility to regrow, as most of them are resprouting species. Thinning follows a scheme of extraction belts and interbelts, aligning more closely with a "mechanical thinning" approach, specifically "belt thinning" (*sensu* [30]).

In Chucao, the historical thinning type has been constant selection thinning of low intensity. Based on preliminary studies, three events of medium/high extraction (from 1956 to 1961; from 1967 to 1977, and from 1990 to 1997) were recorded. The current vegetation consists of individuals of *Nothofagus antarctica* (ñire), *N. dombeyi* (coihue), *Nothofagus pumilio* (lenga), *Diostea juncea* (retamo), *Schinus patagonicus* (laura), *Austrocedrus chilensis* (ciprés de la cordillera), *Discaria chacaye* (espino negro), *Lomatia hirsuta* (radal), *Embothrium coccineum* (notro), and *Maytenus boaria* (maitén), among others. At this site, the thinning observed resembles a "selection thinning", primarily targeting the removal of dominant trees, either for harvesting large timber or for low-intensity wood extraction, consistent with "low thinning".

2.3. Environmental characterization at site and microsite levels

To conduct a macro and microclimatic characterization at each study site, automatic weather stations (two Davis Vantage Pro 2 and/or HOBO Weather Stations) were installed with a temporal recording interval of 1 hour for the variables (see below) during the 2018–2019 season. The Davis Vantage Pro 2 weather station operates reliably within a temperature range of –40 °C to +65 °C, with a typical temperature accuracy of ± 0.2 °C and relative humidity accuracy of ± 2 % across the 0-100 % RH range. The HOBO Weather Station operates within a similar temperature range (–20 °C to +70 °C) and provides temperature accuracy up to ± 0.21 °C and RH accuracy of ± 2.5 % (10–90 % RH).

Additionally, at the Foyel site, macro meteorological data were recorded at a third location (Ridge Foyel), situated on the ridge between the north and south slopes. In conjunction with the weather station measurements, during the mentioned seasons, data on ambient temperature and relative humidity (microclimate) were collected in at least one plot for each thinning treatment at North and South Foyel using thermo-hygrometers (Hobo H8, Onset Computer Corporation, Bourne, MA). The internal temperature sensor provides an accuracy of ±

Table 1. Main characteristics of the studied sites. References: *Mean DBH*= mean diameter at breast height (± *standard deviation*; cm); m. a. s. l. = meters above sea level.

Site name	Main species composition	Mean basal area (m^2 ha^{-1})	Latitude	Longitude	Mean site altitude (m a. s. l.)	Mean DBH (cm)	Dominant height (m)
North Foyel	*N. antarctica* *A. chilensis* *D. juncea* *S. patagonicus* *D. chacaye* *F. imbricata* *L. hirsuta* *E. coccineum* *M. boaria*	34.8	41° 38' 54.6'' S	71° 30' 31.4'' W	800	5.62 (4.92)	3.54
South Foyel	*N. antarctica* *D. juncea* *S. patagonicus* *L. hirsuta* *E. coccineum*	46.7	41° 38' 49.7'' S	71° 30' 4.9'' W	760	6.08 (3.18)	4.38
Chucao	*N. antarctica* *N. dombeyi* *N. pumilio* *D. juncea* *S. patagonicus* *A. chilensis* *D. chacaye* *L. hirsuta* *E. coccineum* *M. boaria*	21.9	41° 43' 41.9'' S	71° 26' 40.3'' W	862	14.5 (7.80)	6.90

0.4 °C (in high-resolution mode) over the typical operating range. The relative humidity sensor offers an accuracy of ± 3 % RH from 0 °C to + 50 °C, with a full measurement range from 0 to 100 % RH. The thermohygrometers were mounted at 1.5 meters above the ground, in the centre of the strip per thinning treatment, with a temporal recording interval of 1 hour for the variables. All sensors were factory-calibrated and installed following standardized microclimate monitoring protocols (e.g., [31].

Based on the location of the sampling sites within the available ERA5 grid cells for the study seasons (2017–2018 and 2018–2019), one reanalysis dataset was used for all sites in Foyel and a second one for the Chucao site. One important aspect to consider is that ERA5 reanalysis data are referenced to Coordinated Universal Time (UTC), whereas local weather stations record data in official Argentine time (UTC–3). This three-hour difference can produce an apparent shift in the time of day when maximum or minimum temperatures are recorded. This offset was considered when interpreting differences in the daily temperature synchronization between the two datasets. Vapor pressure deficit (VPD, kPa) was estimated according to [32].

2.4. Statistical analysis

The macro and micro meteorological time series underwent analysis employing the wavelet transform [33], with the complex Gabor atom [34] serving as the wavelet function (Supplementary material 1). The Gabor transform was selected over other signal processing methods (e.g., Fourier or low-pass filters) due to its ability to simultaneously preserve time and frequency resolution, which is essential for characterizing daily cycles of microclimatic variability. This transform reduces edge effects and maintains localized temporal features, making it suitable for detecting phase shifts and amplitude differences linked to forest thinning and microsite conditions. Additionally, it acted as a band-pass filter, extracting the 24-hour daily cycles while eliminating interference from seasonal or lower-frequency variations. Simultaneously, it was employed as a low-pass filter to estimate the mean of meteorological variables, excluding frequencies higher than 1/24 hours.

This approach is in line with previous studies using wavelet-based techniques for environmental signal denoising and filtering, such as those described by [35]. Moreover, our attention to measurement frequency and instrument accuracy aligns with metrological practices on uncertainty evaluation in sensor calibration, as recently addressed by [36]. Comparisons of mean, amplitude, and phase estimations for daily air temperatures, relative humidity and VPD were conducted across meteorological weather stations and thermohygrometers, leading to conclusions about the representation of this variability in relation to treatments and the variability within and between meteorological data time series. The utilization of a Gabor atom with a wide window ensured that the estimated parameters were smooth, facilitating result interpretation.

To calculate confidence intervals, a series of Monte Carlo simulations was performed at each convolution step, varying the phase, amplitude, and mean values to estimate the standard deviation around the mean. In this procedure, samples were drawn from a normal distribution with four times the standard deviation of the previous time step (proposal distribution). Samples were then either accepted or rejected, based on comparisons with the target distribution. For each Monte Carlo iteration, a sample was drawn from the proposal distribution, and a random value was generated from a uniform distribution. The ratio of the probability density function (PDF) of the target distribution to that of the proposal distribution (evaluated at the proposed sample) was compared with the random value. If the ratio exceeded the random value, the sample was accepted; otherwise, it was rejected. This process continued until 300 accepted samples were obtained, providing an approximate distribution for each parameter (mean, amplitude, or phase).

These distributions were then used to compute the 95 % confidence intervals across the entire time series.

Once the confidence intervals for each individual time series were calculated, the results were aggregated for the same treatment and location by computing the median. For each date with valid data, the minimum of the lower confidence intervals and the maximum of the upper confidence intervals were also compiled. This method allowed us to establish the confidence intervals for the median of each treatment by aggregating the extreme values across all dates with valid data.

2.5. Comparison between sites, meteorological stations and thermohygrometers

To identify potential differences between time series, we visually inspected the superimposed time series of the nine estimated variables: mean, amplitude, and phase for mean air temperature, air relative humidity, and vapor pressure deficit. This analysis aimed to pinpoint specific moments when the mean, amplitude, or phase of these variables differed among weather stations and/or thermohygrometers, determining when a time series exhibited significantly higher or lower values compared to others, and when these changes occurred. At each point in time, differences were deemed statistically significant if the median of a given time series for any treatment or location fell outside the confidence interval of the time series it was being compared to.

To estimate the degree of similarity in temporal behaviour, the Pearson Correlation Coefficient (r) was calculated for each variable analysed. This analysis was conducted between meteorological stations, between treatments within the same site, between sites with the same treatments (using thermohygrometers), and between all weather stations' time series and the global ERA5 reanalysis data per site (see below, [37]). Confidence intervals (CIs) for r were determined using the Fisher transformation [38]. Specifically, r values were computed for the meantime series, as well as for the upper and lower bounds of the intervals of each series, yielding a total of nine CIs per comparison. To ensure a conservative estimate, the highest of the nine upper bounds was taken as the upper limit of the final CI, and the lowest of the nine lower bounds was chosen as the lower limit.

The ERA5 reanalysis dataset, with its high spatial (~ 31 km) and hourly temporal resolution, offers consistent and reliable data on key climatic variables, such as air temperature, relative humidity, and vapor pressure deficit, enabling analysis across scales, from global to site-specific, and supporting the study of climatic impacts on forest thinning practices.

3. RESULTS

3.1. Climatic patterns across sites, and their relationship with in situ measurements and global models

3.1.1. Temperature

Mean temperature across the different sites (Figure 1 a) showed significant differences. Chucao exhibited the highest mean temperature and a more consistent pattern compared to the Foyel site/locations. Within Foyel, the highest mean temperatures were recorded at the Ridge, followed by the North and South locations. These differences were more pronounced during January and February, when temperatures at Ridge Foyel were clearly higher. After this period, South and North Foyel consistently showed higher temperatures than Ridge Foyel.

ERA5 reanalysis slightly underestimated the mean temperatures in Chucao and, except for mid-January, generally overestimated the values in Foyel, with the largest discrepancies in Ridge Foyel. However, these differences remained within the range of variations observed among the Foyel weather stations (Figure 1 a).

Correlation analysis (Supplementary material 2) confirmed significant correlations across all-time series, with confidence intervals clearly different from zero. In the case of Foyel, correlations were exceptionally high (> 0.99) among the three locations, reflecting strong internal consistency. Correlations between these locations and Chucao were much weaker (~ 0.27). It is worth noting that the ERA5 time series for the different sites (Foyel and Chucao) were highly correlated with each other (0.9988), but their correlations with *in situ* data were very weak (~ 0.26), highlighting greater heterogeneity in locally recorded temperatures compared to ERA5 predictions.

Temperature amplitude (Figure 1 d) was highest and nearly constant during summer (January and February). Amplitude values were more variable in Foyel than in Chucao. Within the Foyel locations, North and Ridge showed significantly higher amplitudes than South, which had the lowest amplitudes, indicating a more thermally stable environment. Amplitudes in Chucao were the highest and most homogeneous between mid-January and mid-February, coinciding with the driest period (Figure 1 b).

The ERA5 model consistently underestimated temperature amplitude for all sites and conditions, failing to capture the observed extremes. Correlation analysis (Supplementary material 2) showed significant correlations across all-time series. However, unlike mean temperature, several amplitude correlations were negative. Within the Foyel locations, correlations remained high (> 0.99), but correlations between these and Chucao were weaker (~ 0.34).

Temperature phase (Figure 1 g) showed site-dependent variation in the timing of the daily maximum temperature, with differences of 1–2 hours between sites and locations, and up to 3 hours between weather station data and ERA5. North Foyel consistently exhibited the latest daily maximum temperature, followed by Chucao, South Foyel and Ridge Foyel. This pattern remained stable throughout the study period.

ERA5 showed significant discrepancies in the timing of the maximum temperature compared to the weather station data, which is consistent with Argentina's time zone being approximately two hours ahead of solar time in the region, similar to the average phase difference observed in the station data.

Correlation analysis of phase shifts (Supplementary material 2) indicated significant correlations across all-time series, with confidence intervals clearly different from zero. However, as with amplitude, some correlations were negative. Correlations within the Foyel locations were consistently high (> 0.99), while correlations between these locations and Chucao were weaker (0.27). ERA5 time series across sites were highly correlated with each other (0.9988), but showed predominantly negative correlations with *in situ* data. Moderate negative correlations were observed for Foyel (–0.42), while Chucao showed weaker positive correlations (0.2724).

3.1.2. Air relative humidity

Mean relative humidity (Figure 1 b) was generally higher in Foyel (regardless of the specific location) than in Chucao. Within Foyel, North Foyel recorded the highest values, followed by Ridge Foyel and South Foyel, except in early February, when

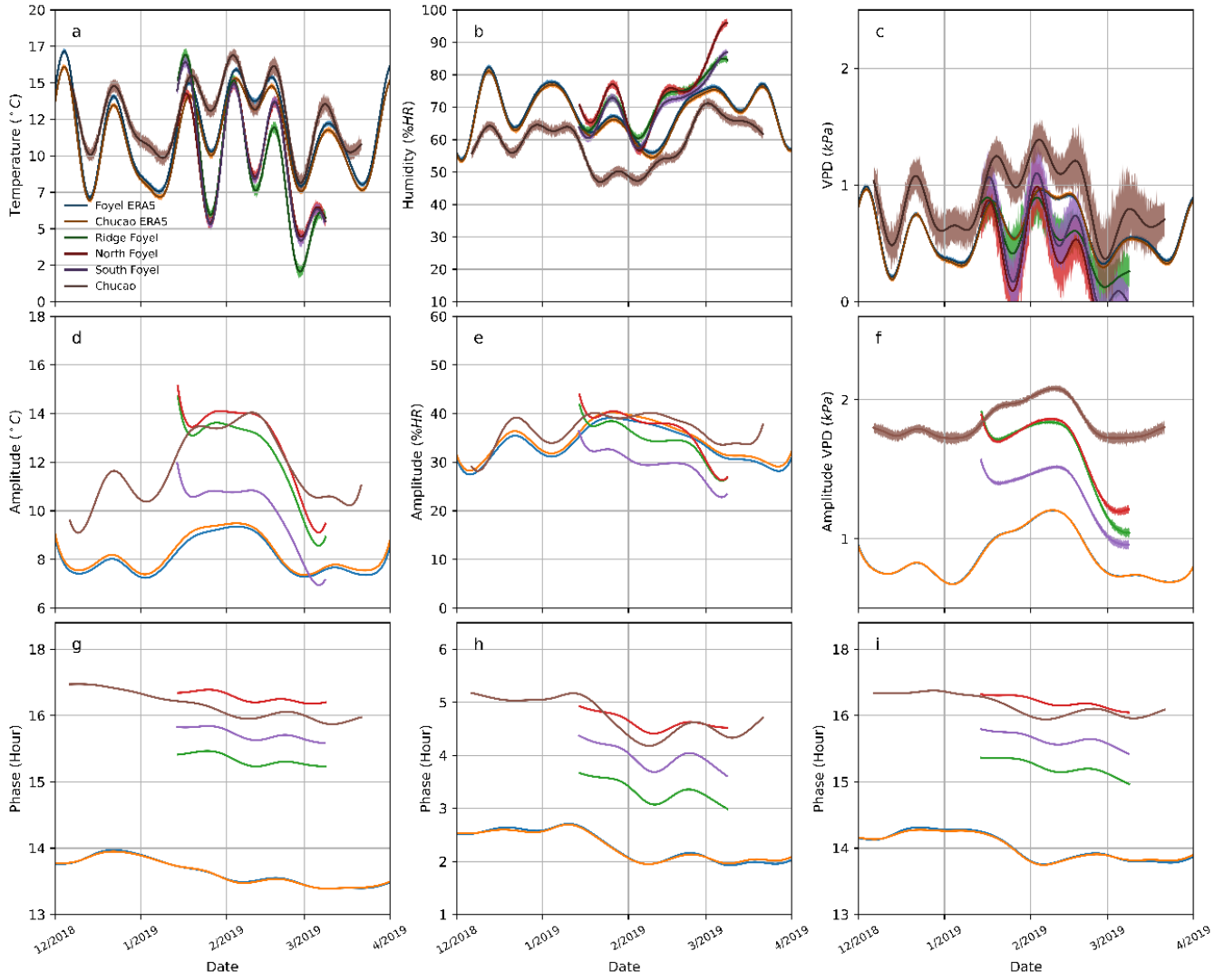

Figure 1. Filtered time series of temperature, relative humidity, and vapor pressure deficit measurements from the Foyel (North, South, and Ridge) and Chucao weather stations, compared with ERA5 reanalysis global model data for the same location. The first row (Panels a, b, c) displays the moving average of the daily mean, calculated using the Gabor wavelet. The second row (Panels d, e, f) shows the amplitude, and the third row (Panels g, h, i) illustrates the phase, represented as the hour of the day when the maximum occurs. The blue and yellow lines represent ERA5 estimations for each location.

Ridge Foyel registered the highest humidity. A notable decrease in mean relative humidity occurred from mid-January to early February, followed by a subsequent increase. Chucao experienced a more pronounced decline during March compared to the other site/locations.

ERA5 overestimated mean relative humidity at Chucao, but underestimated it at all Foyel locations. Discrepancies were smaller for North and South Foyel from mid-January to early February.

Correlation analysis (Supplementary material 2) showed significant correlations in all-time series, with confidence intervals clearly distinct from zero. Within Foyel, correlations among the different weather station records were exceptionally high (> 0.99), but much lower when comparing different sites (~ 0.27). ERA5 data were highly correlated between sites (0.9988), but showed weaker or even negative correlations with *in situ* data (−0.20 for Foyel and ~ −0.12 for Chucao).

Relative humidity amplitude (Figure 1 e) was highest at North Foyel, followed by Ridge Foyel and South Foyel. North and Ridge Foyel showed similar and higher amplitudes than South Foyel, which consistently exhibited the lowest values. Chucao had intermediate amplitude values between those of North and Ridge Foyel, with its highest values observed from mid-February onward. Amplitudes in Chucao were lower than at the Foyel locations.

ERA5 predictions were closest to in situ observations in North Foyel, but it overestimated amplitudes for Ridge and South Foyel. Differences between ERA5 and weather station data were less pronounced in Chucao.

Correlation analysis (Supplementary material 2) confirmed significant correlations across all-time series, with confidence intervals clearly different from zero. Within each site, correlations remained high (> 0.99), while correlations between sites were much lower (~ 0.34). ERA5 time series were highly correlated across Foyel locations (0.9988) but showed mostly negative correlations with *in situ* data. The strongest negative correlations were observed between ERA5 reanalysis data and the different Foyel locations (−0.74), compared to ERA5 and Chucao (−0.51).

Relative humidity phase (Figure 2 h) followed a similar pattern to temperature phase, with differences among the Foyel locations. Maximum relative humidity occurred earlier (~ 3:30

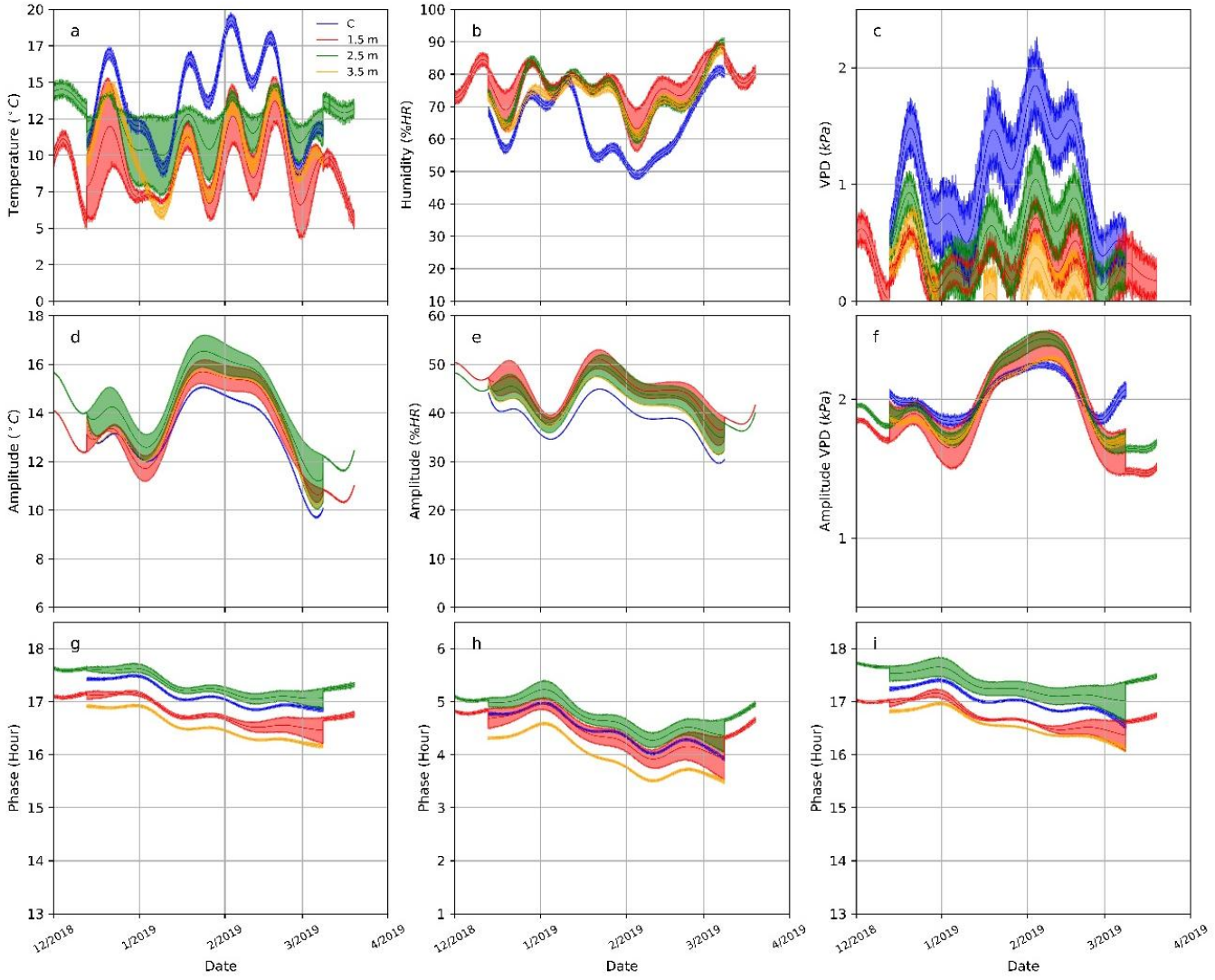

Figure 2. Filtered time series of temperature, relative humidity, and vapor pressure deficit measurements from the North Foyel thermohygrometers. The first row (Panels a, b, and c) presents the moving average of the daily mean, calculated using the Gabor wavelet. The second row (Panels d, e, and f) depicts the amplitude, and the third row (Panels g, h, and i) shows the phase as the hour of the day when the maximum occurs. References: 1.5 m = plots with 30 % of thinning intensity, leaving a 3.0 m space for intact vegetation on the sides; 2.5 m = plots with 50 % of thinning intensity, with the remaining vegetation being 2.0 m wide; 3.5 m = plots with 70 % of thinning intensity, with the remaining vegetation being 1.0 m wide; C = control plot, vegetation was left uncut (0 % removal).

A.M.) at Ridge Foyel, followed by South Foyel, Chucao, and North Foyel, with differences of approximately three hours. ERA5 estimated maximum relative humidity times to be 1–3 hours earlier than the weather station data, regardless of the site.

Correlation analysis of phase shifts (Supplementary material 2) showed significant correlations in all-time series, with confidence intervals clearly distinct from zero. Correlations within the Foyel locations were consistently high (> 0.99), while correlations between these locations and Chucao were lower (~ 0.41). ERA5 time series across sites were highly correlated (0.9972), but correlations with *in situ* data were weaker, with moderate correlations for Foyel (~ 0.42) and virtually no correlation for Chucao (0.0037).

3.1.3. Vapor pressure deficit (VPD)

Mean VPD (Figure 1 c) was consistently higher in Chucao than at the Foyel locations throughout the entire study period, with particularly pronounced differences during January and February. Within Foyel, VPD values were similar across all sites.

ERA5 underestimated the mean VPD in Chucao and overestimated it at the Foyel locations, with the greatest discrepancies in North and South Foyel, while Ridge Foyel showed better agreement.

Correlation analysis (Supplementary material 2) revealed significant correlations in all-time series, with confidence intervals clearly distinct from zero. Correlations within the different Foyel locations were very high (> 0.99), indicating strong internal consistency, while correlations between Foyel (regardless of location) and Chucao were much lower (~ 0.27). ERA5 time series were highly correlated across sites (0.9988), but correlations with *in situ* data were weaker, with slightly higher (though still low) correlations for Foyel (~ 0.231) than Chucao (0.1485).

VPD amplitude (Figure 1 f) was higher at the Foyel locations than in Chucao throughout the study period, although the highest absolute values were recorded in Chucao. North and Ridge Foyel showed similarly high amplitudes compared to South Foyel, which consistently displayed the lowest amplitude,

consistent with a more stable and sheltered environment. ERA5 underestimated the VPD amplitude at all Foyel locations and showed larger discrepancies in Chucao than in Foyel.

Correlation analysis (Supplementary material 2) confirmed significant correlations across all-time series, with confidence intervals clearly distinct from zero. Correlations among the Foyel locations remained high (> 0.99), while correlations between these locations and Chucao were around 0.34. The ERA5 time series between the sites (Foyel vs. Chucao) were strongly correlated (0.9988), but correlations with *in situ* data were predominantly negative, with stronger negative correlations for Foyel (−0.73) than for Chucao (−0.2412).

The phase of Vapor Pressure Deficit (VPD) (Figure 1 i) followed similar trends to the temperature phase, showing variation in the time of day when the VPD maximum occurred. Differences of 1–2 hours were observed between locations/sites, and approximately 3 hours between weather station data and ERA5 reanalysis. During the study period, North Foyel exhibited the latest daily maximum VPD, followed by Chucao (with similar timing), South, and Ridge Foyel. This pattern remained consistent across sites and locations. ERA5 consistently predicted earlier maximum VPD (1–3 hours earlier) than those observed by the weather stations, regardless of locations/site.

Correlation analysis of phase shifts (Supplementary material 2) showed significant correlations across the time series, with some negative values. Correlations within the Foyel locations were consistently high (> 0.99), while correlations between sites were lower (~ 0.28). ERA5 time series across sites were highly correlated (0.9975), but correlations with local data were weaker, with moderate correlations for Foyel (~ 0.41) and low correlations for Chucao (~ 0.2354).

3.2. Effect of thinning treatments on microclimatic conditions

Thermohygrometric data across the different thinning intensity treatments in North and South Foyel showed significant differences in mean air temperature, relative humidity, VPD, and their respective amplitudes and phases (Figure 2 and Figure 3). Despite these differences, variation patterns were consistent across all treatments and locations, as visually observed in the aforementioned figures and supported by the correlation analysis

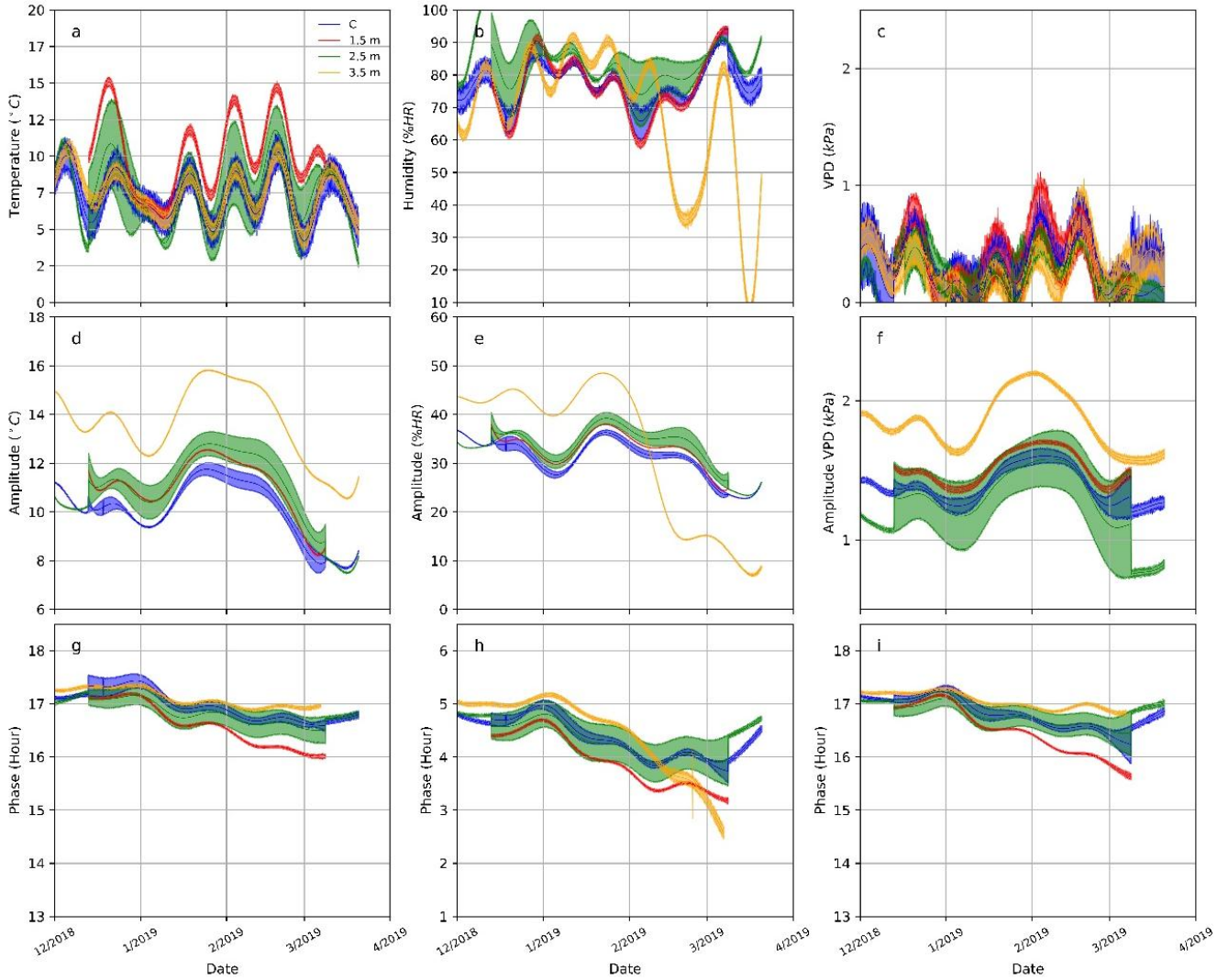

Figure 3. Filtered time series of temperature, relative humidity, and vapor pressure deficit measurements from South Foyel thermohygrometers. The first row (Panels a, b, and c) presents the moving average of the daily mean, calculated using the Gabor wavelet. The second row (Panels d, e, and f) depicts the amplitude, and the third row (Panels g, h, and i) shows the phase as the hour of the day when the maximum occurs. References: 1.5 m = plots with 30 % of thinning intensity, leaving a 3.0 m space for intact vegetation on the sides; 2.5 m = plots with 50 % of thinning intensity, with the remaining vegetation being 2.0 m wide; 3.5 m = plots with 70 % of thinning intensity, with the remaining vegetation being 1.0 m wide; C = control plot, vegetation was left uncut (0 % removal).

(Supplementary material 3) between treatments within the same location and between identical treatments across locations. The results for each meteorological variable are described below.

3.2.1. Temperature

In North Foyel, mean air temperature (Figure 2 a) was higher and more stable across dates (narrower confidence intervals) in the Control treatment (C) compared to the thinning treatments. In the intermediate thinning treatment (2.5 m strip width), wider confidence intervals were observed, indicating greater variation between dates. All treatments followed a similar general pattern, with the largest discrepancies between the Control and the thinned treatments occurring during the warmer months (mid-January and March).

Daily temperature amplitude (Figure 2 b) was lower in the Control than in other treatments, particularly from mid-January to March. Regarding the temperature phase (Figure 2 g), peak temperatures varied by treatment, with the highest thinning intensity (3.5 m strips) reaching the daily temperature peak earliest (around 4:30 PM), and the intermediate thinning (2.5 m) peaking latest (around 5:30 PM).

In South Foyel, the lowest thinning intensity (1.5 m strips) showed significantly higher mean temperatures, differing significantly only from the Control (Figure 3 a). The other treatments exhibited similar mean temperatures. Temperature amplitude (Figure 3 d) was highest in the highest thinning intensity treatment (3.5 m), followed by the narrower strip widths, which were similar to each other. As in North Foyel, the Control had the lowest amplitude. Regarding temperature phase (Figure 3 g), the different treatments showed similar values until mid-January, when the 3.5 m treatment showed a delay of 30 minutes to 1 hour, relative to the 1.5 m treatment. That is, on this site, the highest thinning intensity treatment had the latest daily temperature peak, opposite to what was observed in North Foyel. The intermediate (2.5 m) and Control treatments had intermediate peak timing between the two extremes of thinning intensity.

Correlation coefficients indicated significant variability in temperature metrics between treatments and sites (Supplementary material 3). In North Foyel, strong positive correlations were observed between the Control and the highest thinning intensity (3.5 m), while correlations between the Control and intermediate intensities (1.5 m and 2.5 m) were moderate to low. In South Foyel, correlations between treatments were generally higher, with particularly strong values between the Control and 3.5 m, similar to North Foyel. For temperature amplitude, the highest correlations in North Foyel were found between the two lowest thinning intensities (1.5 m and 2.5 m). For temperature phase, correlations were moderate to high within each site, with the highest values between the Control and the 2.5 m treatments in South Foyel.

3.2.2. Air relative humidity (RH)

In North Foyel, the Control treatment (C) consistently showed lower relative humidity compared to the thinning treatments, with statistically significant differences for most of the study period (Figure 2 b). Thinning treatments did not differ significantly from each other in terms of the mean relative humidity. The amplitude analysis (Figure 2 e) revealed comparable values across treatments, except for the Control, which showed lower amplitudes. A steady decrease in humidity amplitude was observed during January, followed by a brief increase and a gradual decline through April. Regarding phase, the highest thinning intensity treatment (3.5 m strips) reached its humidity peak one hour earlier than the 2.5 m treatment, with the 1.5 m and Control treatments showing intermediate values, statistically distinct from the extremes.

In South Foyel, the mean relative humidity values were similar across the treatments, except for the 3.5 m treatment, which showed a more variable pattern. Significant differences were observed during January and from mid-February to April, with this treatment showing a notable reduction in mean humidity toward the end of the study period. Overall, the 1.5 m and Control treatments were more similar to each other than to the others. Relative humidity amplitude was highest for the 3.5 m treatment until early February, after which it showed the lowest amplitude (Figure 3 e). For phase (Figure 3 h), the 3.5 m treatment showed a statistically significant delay in its humidity peak compared to the other treatments until the end of January. Toward the end of the study, both the 3.5 m and 1.5 m treatments reached their peak one hour later than the Control and 2.5 m treatments.

Correlation analysis showed strong correlations for mean RH values in several treatment pairs, particularly between the Control and the 3.5 m treatment in North Foyel. Amplitude correlations were also highest between the Control and the 3.5 m treatment at this site, while phase correlations were generally moderate to high within each site.

3.2.3. Vapor pressure deficit (VPD)

Driven by higher temperatures, in North Foyel, the Control treatment (C) showed the highest mean VPD, followed by the 2.5 m, 1.5 m, and 3.5 m thinning treatments (Figure 2 c). All treatments displayed similar variation patterns. The amplitude analysis showed clear differences between all thinning treatments and the Control, with the latter displaying higher amplitudes at the beginning and the end of the study period. All treatments reached peak VPD amplitudes during February (Figure 2 f). Regarding phase, the 2.5 m treatment exhibited a significant delay (~ 1 hour) compared to the 3.5 m treatment, while the 1.5 m and the Control treatments also differed significantly, though with smaller delays (Figure 2 i).

In South Foyel, mean VPD values were similar across treatments (Figure 3 c), with comparable variation patterns. The amplitude analysis (Figure 3 f) revealed that the 3.5 m treatment had the highest amplitudes, while the 2.5 m treatment showed the lowest and most variable amplitudes, with no significant differences from the 1.5 m and the Control treatments. These two treatments showed only slight amplitude differences over the course of the study. No significant differences were observed in VPD phase values (Figure 3 i), except for the 3.5 m treatment, which exhibited a slight delay compared to the 2.5 m and the Control treatments in mid-February. The most pronounced discrepancy was observed in the lowest thinning intensity treatment (1.5 m), which reached the daily VPD peak approximately one hour later than the other treatments, from late January to the end of the study.

Correlation analysis indicated strong correlations for mean VPD values between treatments within each site, with the highest correlation observed between the Control and the 2.5 m treatments in South Foyel. Amplitude correlations were strongest among the lower-intensity thinning treatments, such as between 1.5 m and 2.5 m in North Foyel, while phase correlations were moderate but consistent across treatments within each site (Supplementary material 3).

4. DISCUSSION AND CONCLUSIONS

This study demonstrates the significant influence of local topography, vegetation structure, and thinning practices on microclimatic conditions in mixed temperate forests of Northern Patagonia. The key findings highlight the interplay between climatic patterns and site-specific factors, such as altitude, slope exposure, and forest structure. Differences in temperature, relative humidity, and vapor pressure deficit across sites illustrate the critical role of these variables in shaping local climatic variability.

Clear and consistent differences were observed between the South, North, and Ridge Foyel, and the Chucao sites, attributable to altitude and exposure. Ridge Foyel exhibited higher temperatures and thermal amplitudes, with higher VPD values during summer, likely reflecting greater solar exposure. It also showed higher mean temperatures and lower RH, indicating a warmer and drier microclimate. Contrary to expectations, the VPD in Chucao was not consistently lower, despite the dense canopy typically associated with more humid environments [12]. This suggests that factors such as altitude and slope exposure may override canopy effects on VPD under certain conditions, highlighting the complexity of climatic interactions and the need for site-specific investigations. These results are consistent with previous studies documenting temperature and moisture retention variations driven by elevation [39], [40].

The hourly phase differences in maximum air temperature, relative humidity, and VPD among sites further support the influence of topography and orientation, confirming that terrain and exposure strongly shape climate, which is key to understanding vegetation dynamics patterns.

The comparison between climatic reanalysis data and site-specific field measurements revealed that ERA5 underestimated the mean temperatures at some sites (e.g., Chucao) and overestimated them in some Foyel locations, showing low correlation with local station data. ERA5 consistently underestimated both temperature and VPD amplitudes. The hourly phases of the different variables also differed between ERA5 and in situ measurements, confirming the model's lack of accuracy at the site scale. Additionally, ERA5 showed high coherence between sites but low sensitivity to real topographic differences. This demonstrates that widely used global reanalysis models have limitations and do not adequately reflect local climatic heterogeneity, especially in mountainous and structurally complex forest environments, in line with findings by [41]. Reanalysis products, such as ERA5, which combine observations with numerical climate models, have a fixed spatial resolution (~ 30 km for ERA5), limiting their ability to capture complex climates driven by topography, altitude, exposure, and vegetation cover. Authors like [42] emphasized that global models generally smooth climatic gradients in mountainous regions, and that interpolation based on weather stations performs better locally only when station density is high, which is often not the case in remote areas such as Northwestern Patagonia.

Consistent with the observations of this study, [43] validated ERA5-Land (with higher spatial resolution than ERA5), using observations in various mountain regions, and found that, while average temperature aligned reasonably well, relative humidity and VPD showed greater deviations, especially in areas with strong topographic heterogeneity. Likewise, in environments such as the Patagonian Andes, [44] observed that ERA5 captured regional trends adequately but failed to reflect intra-site variability and differences between understory and open areas. In such cases, combining ERA5 with in situ sensors at selected geographic points is key. Another relevant example is the study by [45], where ERA5 was combined with field measurements to model water stress in European temperate forests, highlighting the need to adjust ERA5 VPD estimates to reflect real conditions under the canopy.

Despite the aforementioned limitations, ERA5 remains a useful tool in mountainous areas when combined with local sensors for calibration or bias correction, when used to identify regional patterns and climatic anomalies (e.g., heatwaves or droughts), or when employed in eco-physiological or dendroclimatic models requiring continuous climatic variables over time. According to [46], temperate mountain forests in the Andean region of South America represent one of the largest and most continuous areas of natural deciduous forest globally. Due to their pronounced disturbance regimes and various successional stages, climatic zoning combined with meso- and microclimatic characterization is important for identifying occurrence thresholds of different species.

The results provide partial support to affirm that high vegetation cover generates more stable microclimatic conditions. In general, unthinned (Control) treatments in both sites showed lower daily thermal amplitude, less variability in temperature between dates (confidence intervals around the mean), and greater RH stability compared to thinned treatments. These findings align with previous studies in temperate forests emphasizing the role of closed canopies in buffering temperature and humidity fluctuations [12]-[47]. However, VPD in the Control treatment also showed high confidence intervals around the mean (comparable to thinned treatments) and greater daily amplitudes at certain points in the growing season (beginning and end).

Additionally, variations in the daily phase of climatic curves were observed, especially for temperature and VPD, suggesting differentiation in daily patterns under different canopy conditions. This pattern was also documented by [48], who observed shifts in the timing of the daily thermal peak following thinning treatments.

An important aspect to consider is that the size and shape of canopy openings can influence the degree of microclimatic modification. In this regard, [49] demonstrated that elongated or circular shapes and gaps of 150 and 300 m² generate distinct—though moderate—microclimatic effects in mature forests. While gap shape was not explicitly evaluated in this study, the more intense thinning treatments, equivalent to larger openings, produced greater microclimatic fluctuations, reinforcing the importance of these structural variables.

Nevertheless, the behavior of some treatments was not consistent between sites, providing support to affirm that the interaction between management practices and regional climatic patterns is influenced by topography. Specifically, the 1.5 m treatment in South Foyel exhibited higher mean temperatures and later thermal phases than expected, in contrast with North Foyel. This difference likely reflects factors such as solar exposure and altitude, which have been widely reported as modulators of microclimate in mountainous regions [50], [51]. Consequently, these results reinforce the need to implement adaptive forest management approaches that account for both regional climatic context and microsite-specific conditions. Experiences in temperate regions such as the European Alps and the Pacific Northwest of the U.S. demonstrate the applicability of this approach, integrating silvicultural practices with

objectives of climate resilience, biodiversity conservation, and climate change mitigation [52], [53].

Finally, this study underscores the importance of advancing research that explores the long-term microclimatic effects of thinning, incorporating broader ecological gradients, different sizes, shapes, and spatial orientations of interventions, and technologies such as remote sensing, to develop more effective and scalable management strategies for the conservation and sustainable use of temperate forest ecosystems.

AUTHORS' CONTRIBUTION

Santiago Varela and Octavio Bruzzone contributed to the conceptualization, data curation, formal analysis, methodology, writing of the original draft, and review and editing. Juan Pablo Diez and Mariana Weigandt contributed to the conceptualization, data curation, and writing of the original draft. Emilio Bianchi, Marcos Nacif, and Lucas A. Garibaldi contributed to the conceptualization and review of the original draft.

REFERENCES

[1] T. H. Booth, H. A. Nix, J. R. Busby, M. F. Hutchinson, Bioclim: the first species distribution modelling package, its early applications and relevance to most current MaxEnt studies, Diversity and Distributions, 20(1) (2014), pp. 1–9. DOI: 10.1111/ddi.12144

[2] J. Elith, J. R. Leathwick, Species distribution models: Ecological explanation and prediction across space and time, Annual review of ecology, evolution, and systematics 40(1) (2009), pp. 677-697. DOI: 10.1146/annurev.ecolsys.110308.120159

[3] M. Jarraud, WMO-No. 8, 2008. 8. 372 World Meteorological Organization, Geneva, Switzerland.

[4] R. I. Bertin, Plant phenology and distribution in relation to recent climate change, The Journal of the Torrey Botanical Society, 135(1) (2014), pp. 126-146. DOI: 10.3159/07-RP-035R.1

[5] V. Deblauwe, V. Droissart, R. Bose, B. Sonké, A. Blach-Overgaard, (+ another 5 authors), Remotely sensed temperature and precipitation data improve species distribution modelling in the tropics, Global Ecology and Biogeography 25(4) (2016), pp. 443-454. DOI: 10.1111/geb.12426

[6] Z. Abd Latif, G. A. Blackburn, The effects of gap size on some microclimate variables during late summer and autumn in a temperate broadleaved deciduous forest, Int. Journal of Biometeorology 54 (2010), pp. 119-129. DOI: 10.1007/s00484-009-0260-1

[7] J. Harper, J. White, The demography of plants, Annual review of ecology and systematics (1974), pp. 419-463. DOI: 10.1146/annurev.es.05.110174.002223

[8] G. Aussenac, Interactions between forest stands and microclimate: Ecophysiological aspects and consequences for silviculture, Annals of forest science 57(3) (2010), pp. 287-301. DOI: 10.1051/forest:2000119

[9] P. I. Campanello, M. G. Gatti, A. Ares, L. Montti, G. Goldstein, Tree regeneration and microclimate in a liana and bamboo-dominated semideciduous Atlantic Forest, Forest Ecology and Management 252 (1-3) (2007), pp. 108-117. DOI: 10.1016/j.foreco.2007.06.032

[10] P. De Frenne, J. Lenoir, M. Luoto, B. R. Scheffers, F. Zellweger, (+ another 19 authors), Forest microclimates and climate change: Importance, drivers and future research agenda, Glob. Change. Biol. 27 (2012), pp. 2279-2297. DOI: 10.1111/gcb.15569

[11] C. Daly, D. R. Conklin, M. H. Unsworth, Local atmospheric decoupling in complex topography alters climate change impacts, International Journal of Climatology 30(12) (2010), pp. 1857-1864. DOI: 10.1002/joc.2007

[12] J. Chen, S. C. Saunders, T. R. Crow, R. J. Naiman, K. D. Brosofske, G. D. Mroz, B. L. Brookshire, J. F. Franklin, Microclimate in forest ecosystem and landscape ecology: Variations in local climate can be used to monitor and compare the effects of different management regimes, BioScience 49(4) (1999), pp. 288-297. DOI: 10.2307/1313612

[13] B. Choat, S. Jansen, T. J. Brodribb, H. Cochard, S. Delzon, (+ another 19 authors), Global convergence in the vulnerability of forests to drought, Nature 491(7426) (2012), pp. 752-755. DOI: 10.1038/nature11688

[14] T. Jucker, T. D. Jackson, F. Zellweger, T. Swinfield, N. Gregory, (+ another 14 authors), A research agenda for microclimate ecology in human-modified tropical forests, Frontiers in Forests and Global Change 2 (92) (2020). DOI: 10.3389/ffgc.2019.00092

[15] B. Rewald, C. Ammer, T. Grams, H. Hartmann, G. Hoch, K. M. Keiblinger, A. Malyshev, I. C. Meier, Woody plants and forest ecosystems in a complex world—ecological interactions and physiological functioning above and below ground, Frontiers in Plant Science 11(173) (2020). DOI: 10.3389/978-2-88963-640-2

[16] X. Morin, L. Fahse, H. Jactel, M. Scherer-Lorenzen, R. García-Valdés, H. Bugmann, Long-term response of forest productivity to climate change is mostly driven by change in tree species composition, Scientific reports 8(1) (2018) 5627. DOI: 10.1038/s41598-018-23763-y

[17] W. Thuiller, B. Lafourcade, R. Engler, M. B. Araújo, BIOMOD–a platform for ensemble forecasting of species distributions, Ecography 32(3) 2009), pp. 369-373. DOI: 10.1111/j.1600-0587.2008.05742.x

[18] R. Bertrand, J. Lenoir, C. Piedallu, G. Riofrío-Dillon, P. de Ruffray, C. Vidal, J.-C. Pierrat, J.-C. Gégout, Changes in plant community composition lag behind climate warming in lowland forests, Nature 479 (2011) 517-520. DOI: 10.1038/nature10548

[19] D. U. Hooper, E. C. Adair, B. J. Cardinale, J. E. K. Byrnes, B. A. Hungate, (+ another 5 authors), A global synthesis reveals biodiversity loss as a major driver of ecosystem change, Nature 486 (2012), pp. 105-108. DOI: 10.1038/nature11118

[20] D. A. Coomes, O. Flores, R. Holdaway, T. Jucker, E. R. Lines, M. C. Vanderwel, Wood production response to climate change will depend critically on forest composition and structure, Global change biology 20(12) (2014), pp. 3632-3645. DOI: 10.1111/gcb.12622

[21] T. T. Veblen, R. S. Hill, J. Read J (Eds.) The ecology and biogeography of Nothofagus forests, Yale University Press, 1996.

[22] G. Martínez Pastur, T. Schlichter, S. Matteucci, J. Gowda, A. Huertas Herrera, (+ another 4 authors), Synergies and trade-offs of national conservation policy and agro-forestry management over forest loss in Argentina during the last decade, In: Lorenzo, C. (ed). Latin America in times of global environmental change, The Latin American Studies book series, Springer, Cham, 2020, pp. 135-155. DOI: 10.1007/978-3-030-24254-1_9 ,

[23] V. Rusch, D. López, L. Cavallero, G. Rusch, P. L. Peri, (+ another 5 authors), Un marco ecológico para establecer márgenes de manejo de sistemas silvopastoriles. 1- El caso de ñirantales del norte de la Patagonia, Argentina, Actas VIII Congreso Internacional sobre Sistemas Agroforestales para la Producción Pecuaria y Forestal Sostenible- Tercer Congreso Nacional de Sistemas Silvopastoriles, Ediciones INTA; Peri P. L., INTA; 7 al 9 de mayo 2015; Iguazú (Misiones). [In Spanish]

[24] V. E. Rusch, D. R. López, L. Cavallero, G. M. Rusch, L. A. Garibaldi, J. Grosfeld, P. Peri, Modelo de estados y transiciones de los ñirantales del NO de la Patagonia como herramienta para el

uso silvopastoril sustentable, Ecología Austral 27 (2017), pp. 266278. [In Spanish]
DOI: 10.25260/ea.17.27.2.0.240
[25] V. E. Rusch, S. A. Varela, Bases Para El Manejo De Bosques Nativos Con Ganadería En Patagonia Norte, Parte I Ediciones INTA, Buenos Aires, 2019, p. 160. [In Spanish]
[26] G. C. Gallopín, Adaptive environmental assessment and management, C. S. Holling (ed.); Wiley, Chichester, 1978.
[27] E. Bianchi, R. Villalba, M. Viale, F. Couvreux, R. Marticorena, New precipitation and temperature grids for northern Patagonia: Advances in relation to global climate grids, Journal of Meteorological Research, 30(1) (2016), pp. 38-52.
DOI: 10.1007/s13351-015-5058-y
[28] J. A. Reque, M. Sarasola, J. Gyenge, M. E. Caracterización silvícola de ñirantales del norte de la Patagonia para la gestión forestal sostenible, Bosque 28(1) (2007), pp. 33-45. [In Spanish]
[29] J. Gyenge, M. E. Fernández, M. Sarasola, M. de Urquiza, T. Schlichter, Ecuaciones para la estimación de biomasa aérea y volumen de fuste de algunas especies leñosas nativas en el valle del río Foyel, NO de la Patagonia argentina, Bosque 30(2) (2009), pp. 95-101. [In Spanish]
[30] M. P. Camacho, Técnicas de raleo forestal, Instituto Tecnológico de Costa Rica, Departamento de Ingeniería Forestal, Centro de Investigación Forestal, San José, 1980, 100 pp. [In Spanish]
[31] R. Geiger, R. H. Aron, P. Todhunter, The Climate Near the Ground (7th ed.), Lanham, MD: Rowman & Littlefield Publishers, 2009.
[32] B. E. Ewers, R. A. M. Oren, Analyses of assumptions and errors in the calculation of stomatal conductance from sap flux measurements, Tree Physiology, 20(9) (2000), pp. 579-589.
[33] P. S. Addison, The illustrated wavelet transforms handbook: introductory theory and applications in science, engineering, medicine and finance, CRC press, 2017.
[34] D. Gabor, Theory of communication, Part 1: The analysis of information, Journal of the Institution of Electrical Engineers-part III: radio and communication engineering, 93(26) (1946), pp. 429-441.
[35] D. Stefanutti, V. Bruni, Signal denoising using the Stationary Wavelet Decomposition, Proc. of the IMEKO TC-19 Workshop on Metrology for the Sea, Naples, Italy, 11–13 October 2017, pp. 104-110. Online [Accessed 8 September 2025]
https://imeko.org/publications/tc19-Metrosea-2017/IMEKO-TC19-METROSEA-2017-21.pdf
[36] M. AlOtaibi, M. Zari, M. Alshahrani, A. Aldalbahi, Calibration of an unloaded laboratory oven and the associated uncertainty of measurements, Acta IMEKO, 14(2) 2025, pp. 1-8.
DOI: 10.21014/actaimeko.v14i2.1918
[37] H. Hersbach, B. Bell, P. Berrisford, G. Biavati, A. Horányi, (+ another 10 authors), ERA5 hourly data on single levels from 1940 to present, Copernicus Climate Change Service (C3S) Climate Data Store (CDS), 2023.
DOI: 10.24381/cds.adbb2d47
[38] R. A. Fisher, Frequency distribution of the values of the correlation coefficient in samples of an indefinitely large population, Biometrika, 10 (4) (1915), pp. 507-521.
DOI: https://doi:10.2307/2331838
[39] C. Körner, The use of 'altitude' in ecological research, Trends in Ecology & Evolution, 22(11) (2007), pp. 569-574.
[40] Y. Zhang, et al. Altitudinal patterns of soil microbial biomass and respiration are regulated by plant functional groups in alpine ecosystems, Soil Biology and Biochemistry 119 (2018), pp. 45-51.
[41] W. Xu, X. Lei, S. Chen, T. Yu, Z. Hu, (+ another 8 authors), How Well Does the ERA5 Reanalysis Capture the Extreme Climate Events Over China? Part II: Extreme Temperature, Front. Environ. Sci. 10:921659.
DOI: 10.3389/fenvs.2022.921659
[42] C. Daly, M. Halbleib, J. I. Smith, W. P. Gibson, M. K. Doggett, G. H. Taylor, J. Curtis, P. P. Pasteris, Physiographically sensitive mapping of climatological temperature and precipitation across the conterminous United States, Int. Journal of Climatology, 28(15), pp. 2031-2064.
DOI: 10.1002/joc.1688
[43] J. Muñoz-Sabater, E. Dutra, A. Agustí-Panareda, C. Albergel, G. Arduini, (+ another 12 authors), ERA5-Land: a state-of-the-art global reanalysis dataset for land applications, Earth Syst. Sci. Data, 13, 4349-4383.
DOI: 10.5194/essd-13-4349-2021
[44] J. Fierke, B. Putzenlechner, A. Simon, J. H. Gowda, E. J. Reiter, H. Walentowski, M. Kappas, Modelling microclimatic variability in Andean forests of northern Patagonia, Int. Journal of Biometeorology
DOI: 10.1007/s00484-025-02891-x
[45] Ch. Grossiord, T. N. Buckley, L. A. Cernusak, K. A. Novick, B. Poulter, R. T. W. Siegwolf, J. S. Sperry, N. G. McDowell, Plant responses to rising vapor pressure deficit, Tansley review, New Phytologist 226, pp. 1550-1566.
DOI: 10.1111/nph.16485
[46] A. Simon, J. Fierke, E. J. Reiter, G. A. Loguercio, S. Heinrichs, B. Putzenlechner, N. Z. Joelson, H. Walentowski, The interior climate and its microclimatic variation of temperate forests in Northern Patagonia, Argentina International Journal of Biometeorology 68 (2024), pp. 719-730.
DOI: 10.1007/s00484-024-02617-5
[47] B. Kovács, T. Flora, N. Csaba, P. Ódor, Unfolding the effects of different forestry treatments on microclimate in oak forests: Results of a 4-yr experiment, Ecological Applications 30(2), 2020, e02043.
DOI: 10.1002/eap.2043
[48] S. Maa, A. Concilio, B. Oakley, M. North, J. Chen, Spatial variability in microclimate in a mixed-conifer forest before and after thinning and burning treatments, Forest Ecology and Management 259, pp. 904-915.
DOI: 10.1016/j.foreco.2009.11.030
[49] C. V. Horváth, B. Kovács, F. Tinya, J. Schadeck Locatelli, N. Csaba, (+ another 4 authors), A matter of size and shape: Microclimatic changes induced by experimental gap openings in a sessile oak–hornbeam forest, Science of the Total Environment 873: 162302.
DOI: 10.1016/j.scitotenv.2023.162302
[50] A. W. D'Amato, J. B. Bradford, S. Fraver, B. J. Palik, Effects of thinning on drought vulnerability and climate response in north temperate forest ecosystems, Ecological Applications, 23(8) 2013, pp. 1735-1742.
[51] F. Zellweger, P. De Frenne, J. Lenoir, (+ another 31 authors), Forest microclimate dynamics drive plant responses to warming, Science 15;368(6492), pp. 772-775.
DOI: 10.1126/science.aba6880
[52] M. Lindner, M. Maroschek, S. Netherer, A. Kremer, A. Barbati, (+ another 7 authors), Climate change impacts, adaptive capacity, and vulnerability of European forest ecosystems, Forest Ecology and Management, 259(4) (2010), pp. 698-709. Online [Accessed 8 September 2025]
https://hal.inrae.fr/hal-02669018
[53] T. A. Spies, Ecological concepts and diversity of old-growth forests, Ecology and Society, 23(4) (2018), pp. 14–20.
DOI: 10.1093/jof/102.3.14

Supplementary material 1

Gabor atoms transform detail

The Gabor atom consists of a trigonometric sinusoidal function multiplied by a sliding Gaussian window function (Gabor, 1946), so the estimated amplitude is the result of the convolution between the vector with data and the complex Gabor function:

$$g(t) = a\, \mathrm{e}^{-\frac{(t-t_0)^2}{2\,\sigma^2}}\, \mathrm{e}^{\mathrm{i}\,2\,\pi\,f(t-t_0)}, \quad \text{A(1)}$$

where a is the amplitude, t is the time variable in days, t_0 is the centre or mean time of the function, σ is the standard deviation controlling the spread of the function, f is the frequency, and i is the imaginary unit. At each position in time (t), the amplitude (a) can be estimated as the inner product between the time series R, and the Gabor function ($g(t)$), divided by the square of the norm of the Gabor function:

$$a(t) = \frac{< R, g(t) >}{\|g(t)\|^2}. \quad \text{A(2)}$$

The phase (φ), on the other hand, is the arctangent of the quotient between the imaginary (a_i) and the real (a_r) part of the sinusoidal function:

$$\varphi(t) = \arctan\left(\frac{a_i}{a_r}\right). \quad \text{A(3)}$$

The trigonometric functions were cosines for the real part and sines for the imaginary, with a frequency of 1/day. To transform the phase into day hours, the phase must be divided by 2 π and multiplied by 24. So, the peak of each variable in time was:

$$M(t) = \frac{24\,\varphi(t)}{2\,\pi}. \quad \text{A(4)}$$

To smooth the results, the sliding Gaussian window of the Gabor function had a standard deviation of three days and was slid 15 minutes in each step of the convolution to keep a good time resolution. The mean was computed by applying a low-pass filter, retaining low-frequency variability by removing wavelet components with frequencies exceeding 1/15 days. For the circadian cycle analysis of temperature, relative moisture, and VPD, a 24-hour bandpass Gabor filter was employed, preserving only wavelet components with a frequency of 1/day [1/(24 hours)] throughout the entire time series.

Supplementary material 2

Mean, amplitude and phase Pearson's correlation coefficients (minimum, maximum values) for IC between different meteorological stations and/or ERA5 model for each one of the studied variables (Temperature, Air Relative Humidity and Vapor Pressure Deficit = VPD) at each site.

Meteorological stations	**Temperature**		
	Mean	*Amplitude*	*Phase*
Foyel ERA5-Chucao ERA5	0.9988 (0.9985, 0.9989)	0.9979 (0.9977, 0.9981)	0.9988 (0.9981,0.9989)
Foyel ERA5- Ridge Foyel	0.2567 (0.2218, 0.2908)	-0.6089 (-0.6316, -0.5852)	-0.4038 (-0.4502, -0.3698)
Foyel ERA5- North Foyel	0.2567 (0.2219, 0.2908)	-0.6104 (-0.6330, -0.5867)	-0.4043 (-0.4483, -0.3676)
Foyel ERA5-South Foyel	0.2568 (0.2220, 0.2909)	-0.6134 (-0.6359, -0.5899)	-0.3971 (-0.4433, -0.3622)
Foyel ERA5-El Chucao	0.1903 (0.1546, 0.2254)	-0.1581 (-0.1935, -0.1224)	0.3061 (0.1785,0.3387)
Chucao ERA5-Ridge Foyel	0.2404 (0.2057, 0.2745)	-0.5803 (-0.6042, -0.5554)	-0.4193 (-0.4651, -0.3874)
Chucao ERA5- North Foyel	0.2404 (0.2057, 0.2745)	-0.5821 (-0.6059, -0.5573)	-0.4202 (-0.4632, -0.3853)
Chucao ERA5-South Foyel	0.2405 (0.2057, 0.2746)	-0.5856 (-0.6092, -0.5609)	-0.4126 (-0.4580, -0.3797)
Chucao ERA5-El Chucao	0.1775 (0.1418, 0.2128)	-0.1367 (-0.1723, -0.1007)	0.2814 (0.1520,0.3145)
Ridge Foyel- North Foyel	0.9999 (0.9999, 0.9999)	0.9972 (0.9970, 0.9974)	0.9972 (0.9970,0.9974)
Ridge Foyel – South Foyel	0.9998 (0.9997, 0.9998)	0.9916 (0.9910, 0.9922)	0.9916 (0.9910,0.9922)
Ridge Foyel filo-El Chucao	0.2736 (0.2396, 0.3069)	0.3442 (0.3118, 0.3759)	0.2724 (0.2384,0.3564)
North Foyel – South Foyel	0.9998 (0.9998, 0.9999)	0.9944 (0.9940, 0.9948)	0.9943 (0.9939,0.9948)
North Foyel -El Chucao	0.2735 (0.2395, 0.3068)	0.3442 (0.3118, 0.3759)	0.2724 (0.2384,0.3565)
South Foyel -El Chucao	0.2733 (0.2393, 0.3066)	0.3442 (0.3118, 0.3759)	0.2734 (0.2394,0.3567)
	Air relative humidity		
	Mean	*Amplitude*	*Phase*
Foyel ERA5-Chucao ERA5	0.9993 (0.9988,0.9993)	0.9989 (0.9988,0.9990)	0.9964 (0.9957,0.9966)
Foyel ERA5- Ridge Foyel	-0.2060 (-0.2406, -0.1708)	-0.7415 (-0.7574, -0.7247)	0.4197 (-0.4165,0.4492)
Foyel ERA5- North Foyel	-0.2060 (-0.2406, -0.1708)	-0.7433 (-0.7591, -0.7266)	0.4152 (-0.4270,0.4449)
Foyel ERA5-South Foyel	-0.2061 (-0.2407, -0.1709)	-0.7469 (-0.7626, -0.7304)	0.4112 (-0.4092,0.4410)
Foyel ERA5-El Chucao	-0.1227 (-0.1584, -0.0865)	-0.5306 (-0.5563, -0.5039)	-0.0517 (-0.0879,0.3804)
Chucao ERA5-Ridge Foyel	-0.2013 (-0.2361, -0.1660)	-0.7282 (-0.7448, -0.7106)	0.4744 (-0.4678,0.5021)
Chucao ERA5- North Foyel	-0.2014 (-0.2361, -0.1660)	-0.7300 (-0.7466, -0.7125)	0.4701 (-0.4783,0.4980)
Chucao ERA5-South Foyel	-0.2014 (-0.2361, -0.1660)	-0.7337 (-0.7501, -0.7164)	0.4659 (-0.4607,0.4939)
Chucao ERA5-El Chucao	-0.1170 (-0.1531, -0.0806)	-0.5132 (-0.5396, -0.4859)	0.0037 (-0.0327,0.3330)
Ridge Foyel- North Foyel	0.9999 (0.9999,0.9999)	0.9972 (0.9970,0.9974)	0.9972 (0.9963,0.9974)
Ridge Foyel – South Foyel	0.9998 (0.9997,0.9998)	0.9916 (0.9910,0.9922)	0.9917 (0.9908,0.9923)
Ridge Foyel filo-El Chucao	0.2736 (0.2396,0.3069)	0.3441 (0.3116,0.3758)	0.4137 (0.2015,0.4434)
North Foyel – South Foyel	0.9998 (0.9998,0.9999)	0.9944 (0.9940,0.9948)	0.9945 (0.9930,0.9949)
North Foyel -El Chucao	0.2735 (0.2395,0.3068)	0.3441 (0.3116,0.3758)	0.4132 (0.1999,0.4429)
South Foyel -El Chucao	0.2733 (0.2393,0.3067)	0.3441 (0.3116,0.3758)	0.4126 (0.2033,0.4424)
	VPD		
	Mean	*Amplitude*	*Phase*
Foyel ERA5-Chucao ERA5	0.9992 (0.9988,0.9993)	0.9998 (0.9998,0.9998)	0.9975 (0.9966,0.9977)
Foyel ERA5- Ridge Foyel	0.2312 (0.1963,0.2655)	-0.7352 (-0.7515, -0.7180)	-0.4126 (-0.4721, -0.3723)
Foyel ERA5- North Foyel	0.2313 (0.1963,0.2656)	-0.7365 (-0.7527, -0.7193)	-0.4161 (-0.4703, -0.3703)
Foyel ERA5-South Foyel	0.2314 (0.1964,0.2657)	-0.7390 (-0.7551, -0.7219)	-0.4060 (-0.4638, -0.3632)
Foyel ERA5-El Chucao	0.1587 (0.1226,0.1943)	-0.2388 (-0.2729, -0.2041)	0.2799 (0.1604,0.3131)
Chucao ERA5-Ridge Foyel	0.2213 (0.1857,0.2563)	-0.7323 (-0.7487, -0.7149)	-0.4584 (-0.5158, -0.4201)
Chucao ERA5- North Foyel	0.2214 (0.1857,0.2564)	-0.7335 (-0.7499, -0.7161)	-0.4620 (-0.5139, -0.4182)
Chucao ERA5-South Foyel	0.2215 (0.1858,0.2565)	-0.7358 (-0.7521, -0.7186)	-0.4519 (-0.5076, -0.4112)
Chucao ERA5-El Chucao	0.1485 (0.1124,0.1841)	-0.2412 (-0.2753, -0.2065)	0.2354 (0.1144,0.2695)
Ridge Foyel- North Foyel	0.9999 (0.9999,0.9999)	0.9972 (0.9970,0.9974)	0.9971 (0.9969,0.9974)
Ridge Foyel – South Foyel	0.9998 (0.9997,0.9998)	0.9916 (0.9910,0.9922)	0.9918 (0.9910,0.9924)
Ridge Foyel filo-El Chucao	0.2736 (0.2396,0.3070)	0.3444 (0.3120,0.3761)	0.2801 (0.2462,0.3587)
North Foyel – South Foyel	0.9998 (0.9998,0.9999)	0.9944 (0.9940,0.9948)	0.9943 (0.9939,0.9948)
North Foyel -El Chucao	0.2735 (0.2396,0.3069)	0.3444 (0.3120,0.3761)	0.2800 (0.2461,0.3588)
South Foyel -El Chucao	0.2734 (0.2394,0.3067)	0.3444 (0.3120,0.3761)	0.2810 2472,0.3590)

Supplementary material 3

Mean, amplitude and phase Pearson's correlation coefficients (minimum, maximum values) for IC between thermohydrometers of different locations within North and South Foyel sites for each one of the studied variables (Temperature, Air Relative Humidity and Vapor Pressure Deficit = VPD). References: 1.5 m = plots with 30 % of thinning intensity, leaving a 3.0 m space for intact vegetation on the sides; 2.5 m = plots with 50 % of thinning intensity, with the remaining vegetation being 2.0 m wide; 3.5 m = plots with 70 % of thinning intensity, with the remaining vegetation being 1.0 m wide; C = control plot, vegetation was left uncut (0 % removal); North = North Foyel; South = South Foyel.

Termohygrometers	**Temperature**		
	Mean	*Amplitude*	*Phase*
North C-North 1.5 m	0.6106 (0.4697,0.6330)	0.6624 (0.4929,0.6823)	0.511 (0.4828,0.5460)
North C-North 2.5 m	0.4102 (0.3249,0.5470)	0.6089 (0.4929,0.6313)	0.5105 (0.4824,0.5460)
North C-North 3.5 m	0.9601 (0.9165,0.9954)	0.9952 (0.9700,0.9955)	0.995 (0.9941,0.9954)
North C-South C	0.3921 (0.2617,0.5199)	0.6266 (0.4702,0.6482)	0.5015 (0.4702,0.5282)
North 1.5 m-North 2.5 m	0.9203 (0.9145,1.0000)	0.9971 (0.9377,1.0000)	1 (0.9992,1.0000)
North 1.5 m-North 3.5 m	0.6268 (0.4542,0.6484)	0.6676 (0.4805,0.6873)	0.5114 (0.4840,0.5460)
North 1.5 m-South 1.5 m	0.6463 (0.4449,0.6670)	0.6566 (0.4838,0.6769)	0.5113 (0.4840,0.5460)
North 2.5-mNorth 3.5 m	0.4269 (0.3967,0.5470)	0.6131 (0.4805,0.6353)	0.5108 (0.4834,0.5460)
North 2.5 m-South 2.5 m	0.8765 (0.7411,0.9627)	0.9638 (0.8864,0.9663)	0.96 (0.9561,0.9627)
North 3.5 m-South 3.5 m	0.3742 (0.2161,0.5259)	0.633 (0.4702,0.6544)	0.7214 (0.7017,0.7421)
South C-South 1.5 m	0.4105 (0.3798,0.5199)	0.6225 (0.4614,0.6443)	0.5019 (0.4697,0.5286)
South C-South 2.5 m	0.9244 (0.7218,0.9907)	0.9888 (0.9029,0.9981)	0.9979 (0.9969,0.9981)
South C-South 3.5 m	0.9819 (0.8165,0.9926)	0.9985 (0.9317,1.0000)	0.6444 (0.6073,0.6652)
South 1.5 m-South 2.5 m	0.5714 (0.3624,0.5954)	0.7225 (0.4713,0.7395)	0.4912 (0.4619,0.5259)
South 1.5 m-South 3.5 m	0.3739 (0.2182,0.5259)	0.6249 (0.4702,0.6466)	0.7129 (0.6917,0.7333)
South 2.5 m -South 3.5 m	0.9152 (0.8232,0.9981)	0.9886 (0.9303,0.9981)	0.6378 (0.6087,0.6589)
	Air Relative Humidity		
	Mean	*Amplitude*	*Phase*
North C-North 1.5 m	0.4907 (0.4337,0.5470)	0.5544 (0.4929,0.5791)	0.4691 (0.4162,0.5460)
North C-North 2.5 m	0.9824 (0.9811,0.9969)	0.5664 (0.4929,0.5906)	0.4812 (0.4336,0.5460)
North C-North 3.5 m	0.9767 (0.9749,0.9954)	0.9962 (0.9796,0.9965)	0.9953 (0.9801,0.9961)
North C-South C	0.5109 (0.4512,0.5373)	0.579 (0.4702,0.6027)	0.4787 (0.4214,0.5249)
North 1.5 m-North 2.5 m	0.4888 (0.4606,0.5470)	0.9995 (0.9559,1.0000)	0.999 (0.9807,1.0000)
North 1.5 m-North 3.5 m	0.4847 (0.4563,0.5470)	0.5538 (0.4847,0.5785)	0.475 (0.4463,0.5456)
North 1.5 m-South 1.5 m	0.494 (0.4660,0.5470)	0.5533 (0.4841,0.5780)	0.4807 (0.4522,0.5460)
North 2.5-mNorth 3.5 m	0.996 (0.9868,0.9985)	0.5656 (0.4847,0.5898)	0.4856 (0.4573,0.5456)
North 2.5 m-South 2.5 m	0.5623 (0.5228,0.6056)	0.9619 (0.8957,0.9645)	0.9531 (0.9221,0.9625)
North 3.5 m-South 3.5 m	0.6091 (0.4713,0.6315)	0.5413 (0.4426,0.5666)	0.6676 (0.6036,0.7415)
South C-South 1.5 m	0.5162 (0.4593,0.5424)	0.5784 (0.4618,0.6021)	0.4934 (0.4570,0.5249)
South C-South 2.5 m	0.8266 (0.8147,0.8544)	0.9886 (0.9149,0.9981)	0.992 (0.9686,0.9981)
South C-South 3.5 m	0.7378 (0.6972,1.0000)	0.7752 (0.5441,1.0000)	0.6902 (0.5726,0.7088)
South 1.5 m-South 2.5 m	0.5742 (0.5330,0.6143)	0.6767 (0.4713,0.6959)	0.4192 (0.3541,0.5259)
South 1.5 m-South 3.5 m	0.6156 (0.4713,0.6377)	0.536 (0.4362,0.5615)	0.6753 (0.5942,0.7333)
South 2.5 m -South 3.5 m	0.572 (0.5315,0.8544)	0.7525 (0.5447,0.9981)	0.6224 (0.5739,0.6526)
	VPD		
	Mean	*Amplitude*	*Phase*
North C-North 1.5 m	0.5727 (0.2054,0.5967)	0.6854 (0.4929,0.7042)	0.5123 (0.4842,0.5460)
North C-North 2.5 m	0.9484 (0.6840,0.9969)	0.6473 (0.4929,0.6679)	0.5042 (0.4759,0.5460)
North C-North 3.5 m	0.5491 (0.3350,0.5740)	0.9916 (0.9741,0.9961)	0.9959 (0.9951,0.9962)
North C-South C	0.7545 (0.3785,0.7697)	0.584 (0.4702,0.6074)	0.4915 (0.4623,0.5249)
North 1.5 m-North 2.5 m	0.6808 (0.3503,0.6998)	0.998 (0.9141,1.0000)	0.9999 (0.9992,1.0000)
North 1.5 m-North 3.5 m	0.5521 (0.1983,0.5769)	0.7078 (0.4816,0.7255)	0.5122 (0.4848,0.5456)
North 1.5 m-South 1.5 m	0.7232 (0.3230,0.7401)	0.691 (0.4874,0.7095)	0.5128 (0.4855,0.5460)
North 2.5-mNorth 3.5 m	0.6984 (0.3381,0.7165)	0.6688 (0.4816,0.6884)	0.5039 (0.4763,0.5456)
North 2.5 m-South 2.5 m	0.8626 (0.5295,0.8716)	0.9579 (0.8370,0.9625)	0.9588 (0.9550,0.9625)
North 3.5 m-South 3.5 m	0.3566 (0.2956,0.3925)	0.6162 (0.4698,0.6383)	0.7217 (0.7018,0.7415)
South C-South 1.5 m	0.8794 (0.2488,0.8874)	0.5877 (0.4649,0.6110)	0.4921 (0.4641,0.5249)
South C-South 2.5 m	0.8633 (0.3767,0.8723)	0.9474 (0.8458,0.9981)	0.9977 (0.9970,0.9981)
South C-South 3.5 m	0.6479 (0.3680,0.7820)	0.9962 (0.9378,1.0000)	0.6398 (0.6074,0.6608)
South 1.5 m-South 2.5 m	0.878 (0.5165,0.8861)	0.7829 (0.4713,0.7966)	0.4834 (0.4540,0.5259)
South 1.5 m-South 3.5 m	0.4281 (-0.0111,0.4574)	0.6046 (0.4702,0.6272)	0.7147 (0.6926,0.7333)
South 2.5 m -South 3.5 m	0.5321 (0.2560,0.5992)	0.9578 (0.9362,0.9981)	0.6277 (0.6051,0.6526)